ELSEVIER

Chemical Engineering Journal 80 (2000) 275–282

Chemical Engineering Journal

www.elsevier.com/locate/cej

The hydrodynamics of a hydrocyclone based on a three-dimensional multi-continuum model

A.F. Nowakowski [a], W. Kraipech [a], R.A. Williams [b], T. Dyakowski [a,*]

[a] *Department of Chemical Engineering, University of Manchester Institute of Science and Technology, P.O. Box 88, Manchester M60 1QD, UK*
[b] *Centre for Particle and Colloid Engineering School of Process Environmental and Material Engineering, University of Leeds, Leeds LS2 9JT, UK*

Abstract

The concept and principles of applying a multi-continuum model for calculating a hydrocyclone performance is presented. In this model the carrying liquid is described as one continuum, and each particle fraction, with its characteristic size is described as a separate continuum. Particle–particle and particle–fluid interactions derived from a lubrication theory and a collision theory are discussed. A set of governing partial differential equations consisting of mass and momentum conservation equations together with constitutive expressions is discussed. These equations were discretized by applying an unstructured grid consisting of tetrahedral elements. A numerical solver based on a finite element method combined with a segregated approach is described. The numerical approach is subject to ongoing research.

Keywords: Hydrodynamics; Hydrocyclone; Multi-continuum model

1. Introduction

In most hydrocyclones, solids are fed in through a single inlet located at a cylindrical part. Downstream, a flow pattern adjusts itself to meet the flow conditions existing within a conical shaped region. The velocity difference between the feed slurry and rotating slurry is the source of turbulence generated at the inlet. Particles, entering a hydrocyclone tend to become located close to the wall as a result of the difference between centrifugal force and the pressure gradient. A flow rotation inside a concave wall generates a high turbulence level within a boundary layer. Turbulence and particle collisions are responsible for dispersing particles within the hydrocyclone body.

The flow behaviour close to the inlet has a profound impact on the efficiency of a hydrocyclone, Nonaka and Tashiro [1]. Diffusive mixing in the hydrocyclone propagates the turbulent energy and particles smaller than about 50 μm and with density less than 3000 kg m^{-3} move along with the surrounding fluid elements. Mixing phenomena at the entrance region to the hydrocyclone are neglected in the existing theoretical and numerical models, Dyakowski and Williams [2], Hsieh and Rajamani [3], and Bloor and Ingham [4]. Inlet conditions are simulated by a uniform distribution of tangential and radial velocities along the circumference, and therefore their assumed values are much lower than the real ones.

Particle separation mechanisms have been studied by calculating their trajectories obtained by solving equations of motion in Lagrangian co-ordinates. Deterministic and probabilistic approaches were developed for a low particle concentration, for example by, Averous and Fuentes [5], and Devulapalli and Rajamani [6]. It seems to be very difficult to extend a Lagrangian approach for higher particles concentrations. This would need to take into account the complex physics describing particle–particle interactions.

A multi-continuum model was proposed by Davidson [7] for studying particle concentration profiles within a hydrocyclone. This model can be applied for the whole range of particle concentrations, and is based on the premise that it is sufficient to describe each solid fraction as a continuum, occupying the same region in space. The new 'fluid' consists of many different phases and sometimes its motion can also be described as a mixture. The fact that all phases remain physically separate implies that the motion of each phase has to be constrained by the presence of other phases. The change of each phase in a control macroscopic volume is measured by the volume fraction (the volume of each phase per unit volume of mixture). Therefore, the principal task of the theoretical description is to specify how the different phases interact between themselves.

The aim of this paper is to present an implementation of a multi-continuum model for a three-dimensional (3D)

* Corresponding author. Fax: +44-161-2004399.
E-mail address: tom.dyakowski@umist.ac.uk (T. Dyakowski).

1383-5866/00/$ – see front matter
PII: S1383-5866(00)00102-7

flow simulation within a hydrocyclone. This model should include constitutive equations describing various types of particle–fluid and particle–particle interactions. An analysis of these interactions is discussed. A finite element method is applied for studying a flow within a 3D geometry. The unstructured grids consisting of tetrahedral elements were generated to describe complex inlet geometry. A choice of approximation function for velocity and pressure, which is crucial in implementing the proposed method, is presented.

2. A multi-continuum model

Consider a mixture composed of a Newtonian fluid (denoted by subscript 'f') and the N particle groups (divided according to particle size and/or density) and denoted by subscript 'i'. Here, ensemble averaged mass and momentum conservation equations are presented. Ensemble averaging avoids shortcomings of time and volume averaging, Crowe et al. [8]. The equations presented below are valid under the following conditions:

- carrying fluid is incompressible and flow is isothermal
- particles deformation, break up and coalescence are neglected
- kinetic turbulent energies describe turbulent interactions between all phases

According to Rajagopal and Tao [9] a set of conservation equations is suggested:

Volume continuity equation for solid phases:

$$\partial\alpha_i/\partial t + \mathrm{div}(\alpha_i \boldsymbol{v}_i) = 0 \tag{1}$$

Mass continuity equations for liquid phase:

$$\partial\rho_\mathrm{f}/\partial t + \mathrm{div}(\rho_\mathrm{f}\boldsymbol{v}_\mathrm{f}) = 0 \tag{2}$$

Momentum conservation equations for solid phases:

$$\partial\rho_i\boldsymbol{v}_i/\partial t + \mathrm{div}(\rho_i\boldsymbol{v}_\mathrm{i}\otimes\boldsymbol{v}_i) = \mathrm{div}(\sigma_i) - \boldsymbol{m} + \rho_i\boldsymbol{b}_\mathrm{I} \tag{3}$$

for liquid phase:

$$\partial\rho_\mathrm{f}\boldsymbol{v}_\mathrm{f}/\partial t + \mathrm{div}(\rho_\mathrm{f}\boldsymbol{v}_\mathrm{f}\otimes\boldsymbol{v}_\mathrm{f}) = \mathrm{div}(\sigma_\mathrm{f}) + \boldsymbol{m} + \rho_\mathrm{f}\boldsymbol{b}_\mathrm{f} \tag{4}$$

Kinetic turbulent energy conservation equations for solid phases:

$$\partial\rho_i k_i/\partial t + \mathrm{div}(\rho_i\boldsymbol{v}_i k_i) = \mathrm{div}(B_i) + \beta_i \tag{5}$$

for liquid phase:

$$\partial\rho_\mathrm{f}k_\mathrm{f}/\partial t + \mathrm{div}(\rho_\mathrm{f}\boldsymbol{v}_\mathrm{f}k_\mathrm{f}) = \mathrm{div}(B_\mathrm{f}) + \beta_\mathrm{f} \tag{6}$$

The definitions of averaged liquid and solids densities and linear momenta are given in Appendix A. σ_i and σ_f are the Cauchy stress tensors associated with the fluid continuum and the solid continua, $\boldsymbol{m}$ is the interactions term between the fluid and solid continua, and $\boldsymbol{b}$ is the external force. k_i and k_f are the turbulent kinetic energies of the solid phases and liquid phases.

To solve the above set of equations, the constitutive equations are needed. Here, the discussion of these equations is presented for a mono-dispersed solids ($\rho_i=\rho_\mathrm{s}$, $\boldsymbol{v}_i=\boldsymbol{v}_\mathrm{s}$, where $i=1, 2, 3, \ldots, N$).

The Cauchy stress tensors σ_f, σ_s and the vector $\boldsymbol{m}$ can be split in two parts:

$$\sigma_\mathrm{f} = \sigma_\mathrm{f}^\mathrm{a} + \sigma_\mathrm{f}^\mathrm{t} \tag{7}$$

$$\sigma_\mathrm{s} = \sigma_\mathrm{s}^\mathrm{a} + \sigma_\mathrm{s}^\mathrm{t} \tag{8}$$

$$\boldsymbol{m} = \boldsymbol{m}^\mathrm{a} + \boldsymbol{m}^\mathrm{t} \tag{9}$$

Components with superscript 't' are responsible for momentum transfer between the averaged velocity fields and fluctuations velocity fields.

$$\sigma_\mathrm{f}^\mathrm{a} = [-\alpha_\mathrm{f}P + a_1\mathrm{tr}\mathsf{D}_\mathrm{f}]\boldsymbol{I} + a_2\mathsf{D}_\mathrm{f} + a_0\rho_\mathrm{f}(\boldsymbol{v}_\mathrm{f}-\boldsymbol{v}_\mathrm{s})\otimes(\boldsymbol{v}_\mathrm{f}-\boldsymbol{v}_\mathrm{s}) \tag{10}$$

$$\sigma_\mathrm{s}^\mathrm{a} = [-\alpha_\mathrm{s}P - 1/2\rho_\mathrm{f}\alpha_\mathrm{s}\,\mathrm{d}a_0/\mathrm{d}\alpha_\mathrm{s}|\boldsymbol{v}_\mathrm{f}-\boldsymbol{v}_\mathrm{s}|^2 + a_3\mathrm{tr}\mathsf{D}_\mathrm{s}]\boldsymbol{I} + a_4\mathsf{D}_\mathrm{s} + a_0\rho_\mathrm{s}(\boldsymbol{v}_\mathrm{f}-\boldsymbol{v}_\mathrm{s})\otimes(\boldsymbol{v}_\mathrm{f}-\boldsymbol{v}_\mathrm{s}) \tag{11}$$

P is a Lagrangian multiplier due to the volume additivity constraint ($\alpha_\mathrm{f}+\alpha_\mathrm{s}=1$) and D is a mean rate of strain tensor. The above equations show a Newtonian fluid like structure, with the additional terms induced by virtual mass effect. Due to the viscous dissipation the coefficients $a_0 \geq 0$, $a_2 \geq 0$, $a_4 \geq 0$, $a_1 + 1/3a_2 \geq 0$, $a_3 + 1/3a_4 \geq 0$.

The interaction between phases is postulated to be described by the following expression:

$$\boldsymbol{m}^\mathrm{a} = -P\nabla\alpha_\mathrm{s} - 1/2\rho_\mathrm{f}\,\mathrm{d}a_0/\mathrm{d}\alpha_\mathrm{s}|\boldsymbol{v}_\mathrm{f}-\boldsymbol{v}_\mathrm{s}|^2\nabla\alpha_\mathrm{s} + a_0\rho_\mathrm{f}(\mathsf{D}^\mathrm{f}\boldsymbol{v}_\mathrm{s}/\mathsf{D}t - \mathsf{D}\mathsf{D}^\mathrm{s}\boldsymbol{v}_\mathrm{f}/\mathsf{D}t) + a_5(\boldsymbol{v}_\mathrm{f}-\boldsymbol{v}_\mathrm{s}) \tag{12}$$

where $a_5 \geq 0$, and the volume additivity constraint, the virtual mass effect, and the drag effect are included.

The structure of the terms representing momentum transfer between the averaged velocity fields and fluctuations velocity fields were assumed to be similar to a Boussinesq's model for a single-phase flow.

Terms B_f and B_s are dependent only on the gradients of the kinetic turbulent energy and the terms β_f and β_s are functions of the gradients of the averaged velocities of both phases and the relative velocity between each phase.

For a multi-dispersed mixture the Bagnoldi stresses play an important role in the vicinity of a hydrocyclone, Davidson [7]. A fluid flow within a hydrocyclone has a 3D character and the presence of a strong swirl manifests itself in an anisotropic character of turbulence, and for such a case, a Boussinesq's model is not suitable.

A general approach describing importance of various types of particle–fluid and particle–particle interaction is based on the force balance acting on a solid particle, Roco [10]. The characteristic time scales are obtained from the analysis of the force balance equation. Within a hydrodynamic region these are the viscous liquid–solid (drag) t_d,

Table 1
Time scales for particle interactions in the hydrodynamic range (from Roco [8])[a]

Type of particle interaction	Time scales (t_m) (s)	Comments
Viscous liquid–solid interaction (drag)	$t_d = \frac{4}{3}\frac{sd_s}{C_D\lvert\boldsymbol{v}_L - \boldsymbol{v}_s\rvert} = sd_s^2/18\upsilon_L$ (5a)	Where $C_D = f(Re_s)$
		For $Re_s < 0.1$
	$= \frac{4}{3}\frac{sd_s}{0.44\lvert\boldsymbol{v}_L - \boldsymbol{v}_s\rvert}$ (5b)	For $Re_s > 10^3$
Lubrication	$t_{lub} = \frac{18}{sd_s}\frac{\dot{\lambda}}{\dot{\gamma}}$ (6)	$\dot{\lambda}/d_s = \frac{1-(\alpha^*)^{0.33}}{(\alpha^*)^{0.33}}$, where $\alpha^* = \alpha_{solid}/\alpha_{max}$
Collision	$t_{col} = \frac{4.5}{s\dot{\gamma}}\log_e(\dot{\lambda}/2\dot{k})$ (7)	$\dot{k}$, the particle-surface roughness, $\dot{k} = f(d_s)$

[a] Where C_D is the drag coefficient, d_s is solid particle diameter, Re_s is particle Reynolds number, s is density ratio between solid and liquid, α_{solid} is the total volume fraction of solid, α_{max} is the total volume fraction of solid at maximum packing, $\dot{\gamma}$ is the mean rate of deformation and υ_L is the kinematic viscosity of liquid phase.

lubrication t_{lub} and collision time scale t_{col}, and are given in Table 1. The relation between various time scales has the form:

$$\frac{\left(\frac{1}{t_m}\right)}{\left(\frac{1}{t_n}\right)} = \frac{t_n}{t_m} = N_{i,m} > 1 \quad (13)$$

An interaction mechanism that is characterised by the time scale t_m is more frequent and therefore has a larger distribution to the momentum transfer than another interaction mechanism characterised by the time scale t_n. Eq. (13) defines the particle interaction number, $N_{i,m}$.

3. Case study of time scales

An example of the calculations of time scales was based on the 75-mm diameter hydrocyclone analysed by Rajamani and Milin [11]. The feed slurry is 35% limestone by wt., and the particle size is ranged from 1 to 90 μm. The results obtained in [11] showed very small variations of the gradient dw/dr along the hydrocyclone height. Taking this into account and the zonal hydrocyclone concepts presented by Concha et al. [12], the flow pattern within a hydrocyclone was split into six regions, Fig. 1. Region II (Fig. 1) covers the flow in a cylindrical part below a vortex finder as well as within a conical part. The flow characteristics of each zone are described in Table 2.

The calculated time scales are shown in Tables 3 and 4. It can be seen that the drag time scale, t_d is independent of the volume fraction while the lubrication and collision time scales, t_{lub} and t_{col} are strongly dependent on volume fraction. On the other hand, the lubrication and collision time scales, t_{lub} and t_{col} are independent of the particle size but the drag time scale, t_d is strongly dependent on the particle size.

The results of the prevailing interaction mechanism in each flow are shown in Fig. 2. For the solid concentration below 0.3% by vol., the main mechanism is viscous liquid–solid interaction (drag). The lubrication mechanism

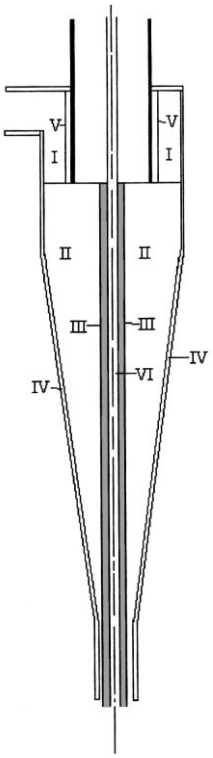

Fig. 1. Zones in a hydrocyclone.

Table 2
The flow characteristics in each zone in hydrocyclone

Zone	Volume fraction	Particle size (μm)	The mean rate of deformation, d$\lvert w^a\rvert$/dr (S^{-1})
I	$\alpha < 0.1$ $0.1 < \alpha < 0.2$ $0.2 < \alpha \leq 0.3$	1–90	80
II	$\alpha < 0.1$ $0.1 < \alpha < 0.2$ $0.2 < \alpha \leq 0.3$	1–90	112
III	$\alpha > 0.3$	1–90	633
IV	$\alpha > 0.3$	1–90	200
V	$\alpha < 0.1$	1–65	420
VI	–	–	–

[a] w denotes the tangential velocity.

Table 3
The drag time scale, t_d of each particle size for all flow zone

Particle size (μm)	$t_d = sd_s^2/18v_f$ (s)
90	1.25×10^{-3}
65	6.0×10^{-4}
45	3.04×10^{-4}
33	1.63×10^{-4}
23	7.94×10^{-5}
16	3.84×10^{-5}
11	1.82×10^{-5}
8	9.6×10^{-6}
4	2.4×10^{-6}
3	1.35×10^{-6}
1	1.5×10^{-7}

is prevalent within the lateral boundary layer and the area near the air-core.

4. 3D numerical algorithm

The philosophy underpinning this work was to avoid the introduction of any numerical technique, which would restrict the geometric flexibility. A finite volume method is not well suited to handle with irregular meshes, which are needed for modelling inlet geometry of hydrocyclones. It should be emphasised that the all-numerical algorithms for flow simulations within a hydrocyclone are restricted to an axi-symmetrical case and for such a case a finite volume technique was applied, Dyakowski and Williams [2]. The need for simulation inlet conditions, as well as the demand for high accuracy, were the main reasons for using the finite element method with the segregated solution algorithm. The segregated solutions are now the preferred method of solution for most Computational Fluid Dynamics solvers. Since, in the finite element technique calculations are performed on element by element basis one can use unstructured meshes. The inherent geometric flexibility permits the easy use of simple Cartesian co-ordinate system. This is considered as a strong advantage particularly in 3D geometry. There is no need for global mappings and global transformation of equations.

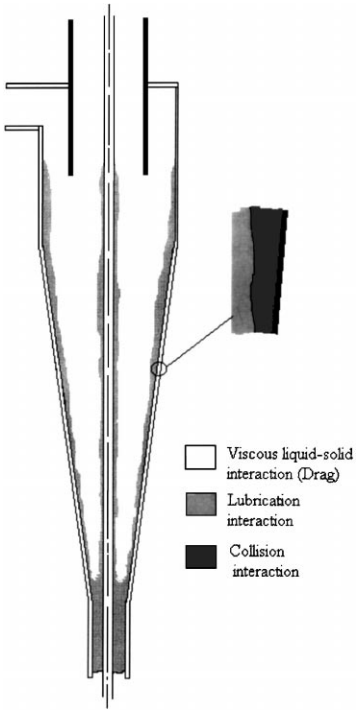

Fig. 2. The main interaction mechanisms in a 75-mm hydrocyclone.

In this work, the unstructured finite element grid, based on tetrahedral elements has been developed. By using these simple shape elements it was possible to accurately represent the computational domain by a finite element mesh. The following methodology was applied when generating a mesh. The computational volume, where possible, was divided into eight-cornered brick elements. A systematic way of creating such elements was devised. The bricks are then divided into five tetrahedral elements. Additional partial refinement of the mesh was made in the boundary region and in the profiled head entry region. A global refinement and adjustment of the mesh is possible in two ways. First of all, global grid parameters and the number of subdivisions

Table 4
The lubrication and collision time scales, t_{lub} and t_{col}

Zone	Solid concentration (volume fraction)	$t_{lub} = \frac{18}{sd_s}\frac{\lambda}{\dot{\gamma}}$ (s)	$t_{col} = \frac{4.5}{s\dot{\gamma}}\log_e(\lambda/2k)$ (s)
I	$\alpha<0.1$	$t_{lub}>0.07504$	$t_{col}>0.17526$
	$0.1<\alpha<0.2$	$0.07504>t_{lub}>0.0426$	$0.17526>t_{col}>0.1635$
	$0.2<\alpha\leq0.3$	$0.0426>t_{lub}\geq0.0268$	$0.1635>t_{col}\geq0.1538$
II	$\alpha<0.1$	$t_{lub}>0.05524$	$t_{col}>0.12327$
	$0.1<\alpha<0.2$	$0.05524>t_{lub}>0.03456$	$0.12327>t_{col}>0.11625$
	$0.2<\alpha\leq0.3$	$0.03456>t_{lub}\geq0.01925$	$0.11625>t_{col}\geq0.109485$
III	$\alpha>0.3$	$t_{lub}<0.0034$	$t_{col}<0.01943$
IV	$\alpha>0.3$	$t_{lub}<0.0107$	$t_{col}<0.0615$
V	$\alpha<0.1$	$t_{lub}>0.01429$	$t_{col}>0.03338$
VI	–	–	–

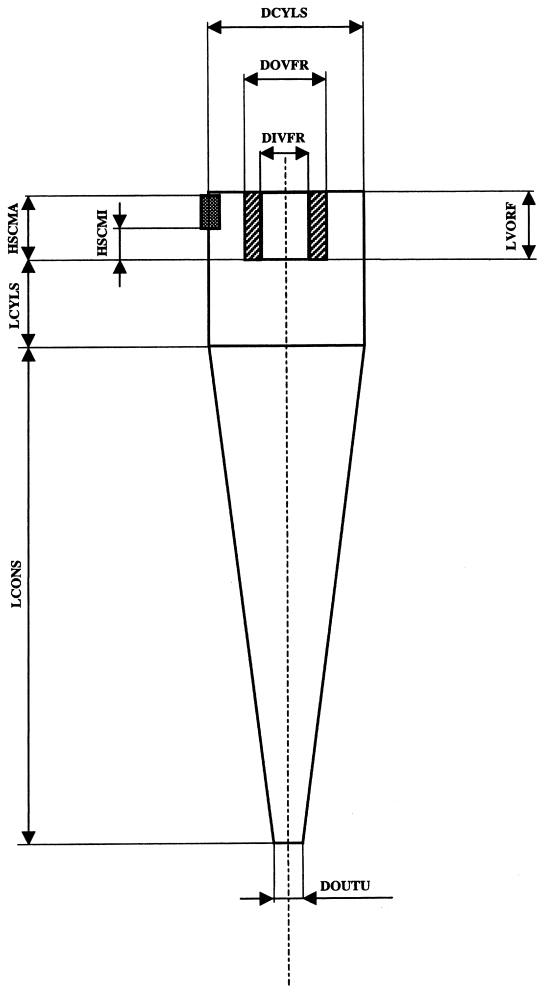

Fig. 3. The dimensions of hydrocyclones which can be changed in computer program.

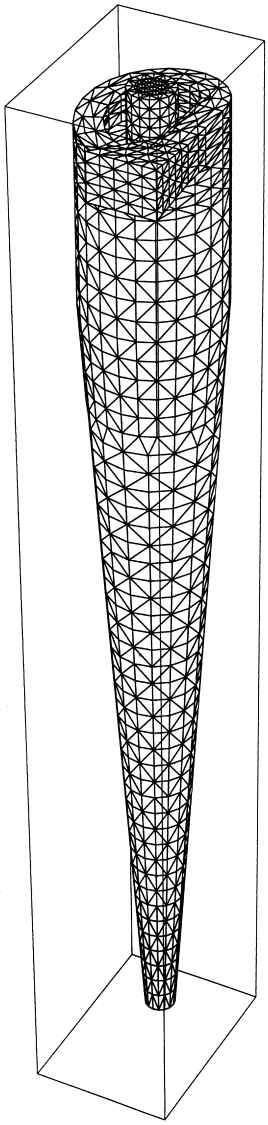

Fig. 4. The unstructured grid consisting of tetrahedral elements within hydrocyclone.

can be changed (Fig. 3). Secondly, subdividing each tetrahedron into 12 smaller tetrahedrons, by first joining the centroid of the large tetrahedron to the vertices and centroids of the faces. This methodology allows one to produce a grid, which applies to hydrocyclones of different dimensions. It was possible to control mesh density and structure. Fig. 4 presents a grid for to 50 mm diameter Mozley hydrocyclone. The mesh comprises the whole hydrocyclone geometry including the head entry section and external part of the inlet feeder orifice (Fig. 5). In this case, the number of elements in the grid was in the order of 26 000, the smallest element being in the central region of the cyclone in the order 1.6 mm. The mesh generation for the cyclone of different dimensions but of the same class is straightforward. One only needs to replace input parameters in the computer program.

In order to introduce an algorithm in compact form the flow model will be treated as a steady-state one-phase case, Gresho [13]. Extension to more general multi-phase turbulent and transient flow will require solving additional

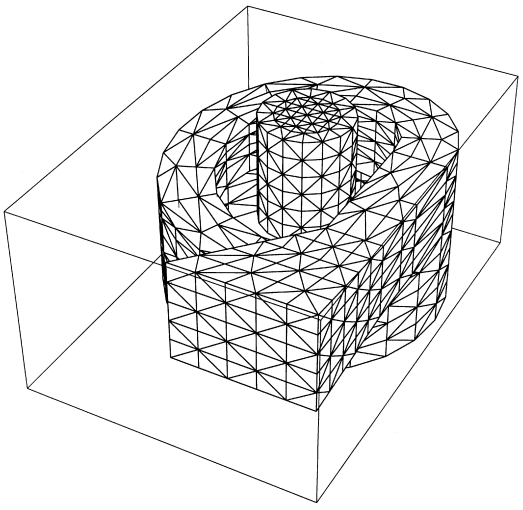

Fig. 5. The grid in the profiled head entry region.

equations, but from the algorithmic point of view this does not change the general philosophy presented below. The weak form of the primitive variables governing equations is of Galerkin's type, Gunzburger [14]. Dependent variables pressure and velocity are approximated by the expansions

$$p^{\mathrm{e}} = \sum_{j=1}^{4} p_j^{\mathrm{e}} \mu_j^{\mathrm{e}} = \boldsymbol{\mu}^T \boldsymbol{p} \tag{14a}$$

$$u_i^{\mathrm{e}} = \sum_{j=1}^{10} u_j^e \varphi_j^e = \boldsymbol{\Phi}^T \boldsymbol{u}_i \tag{14b}$$

where $\boldsymbol{\mu}$ and $\boldsymbol{\Phi}$ and are vectors of interpolation (shape) functions, and $\boldsymbol{u}_i$ and $\boldsymbol{p}$ are vectors of nodal values of velocity components and pressure, respectively. Substitution of Eqs. (14a) and (14b) into a weak form of continuity (1) and momentum (2) equations results in the finite element equations. The derived equations can be written symbolically in matrix form as

$$\begin{bmatrix} \mathbf{K}_{uu} & \mathbf{K}_{uv} & \mathbf{K}_{uw} & -\mathbf{C}_x \\ \mathbf{K}_{vu} & \mathbf{K}_{vv} & \mathbf{K}_{vw} & -\mathbf{C}_y \\ \mathbf{K}_{wu} & \mathbf{K}_{wv} & \mathbf{K}_{ww} & -\mathbf{C}_z \\ \mathbf{C}_x^T & \mathbf{C}_y^T & \mathbf{C}_z^T & 0 \end{bmatrix} \begin{bmatrix} u \\ v \\ w \\ p \end{bmatrix} = \begin{bmatrix} \boldsymbol{F}_x \\ \boldsymbol{F}_y \\ \boldsymbol{F}_z \\ \boldsymbol{b}_{\mathrm{c}} \end{bmatrix} \tag{15}$$

where **K** sub-matrices represent the combined effects of advection and diffusion, **C** matrices are the pressure gradient operators and their transposes; $\mathbf{C}^T$ appearing in the continuity equation is the velocity divergence operators. The vector $\boldsymbol{b}_{\mathrm{c}}$ on the right hand side of the continuity equation represents the contribution to this equation from the non-zero Dirichlet velocity boundary conditions. The vector $\boldsymbol{F}$ contains surface-flux type contributions from the natural boundary conditions as well as a body force.

Two sets of interpolations functions used in equations are of Lagrange type. They cannot be chosen arbitrarily since they have to satisfy compatibility conditions. In order to prevent an over-constrained system of discrete equations, the interpolation used for pressure must be at least one order lower than that used for velocity field, Sani [15,16]. The interpolation functions should satisfy the Ladyzhenskaya–Babuska–Brezzi (LBB) stability condition, Brezzi and Fortin [17]. The Taylor–Hood interpolation functions were used in order to ensure second order accuracy and satisfy the LBB condition, Thatcher [18]. The pressure interpolation function has a linear form and the velocity component interpolation functions are of a quadrilateral form.

As an equation solver the pressure projection algorithm was adopted. The applied algorithm was proposed by Horoutunian et al. [19]. It is a consistent finite element counterpart of the SIMPLER algorithm first introduced by Patankar [20]. The primary variables were de-coupled directly from momentum and continuity Eq. (15) at the discretized level. The algorithm comprises three main steps. They are characterised by generic system $\boldsymbol{Ax}=\boldsymbol{b}$ and are solved sequentially and repeatedly during the course of iteration. At the beginning of a given iteration, an approximation to the pressure is obtained from the solution of a simplified pressure equation using the latest available field variables. The components of the momentum equations are then solved in sequential manner using the most recent field data. Finally, at the end of the whole sequence, the velocity field is corrected to satisfy the discretized continuity equation.

5. Conclusions and further work

A development of a fully 3D model for flow simulations within a hydrocyclone is discussed. Two issues concerned with a practical implementation of this model are addressed:

- The first is concerned with a proper choice of constitutive equations for a multi-continuum model. The postulates presented indicate that both lubrication and particle–particle collision mechanisms are important only for the regions close to the wall. This significantly will reduce the complexity of the constitutive equations.
- The second is focus on the development of a numerical solver. A set of conservation equations was discretized using a 3D grid based on tetrahedral elements. A numerical solver based on a finite element method and a segregated approach is presented in a compact form. The accurate representation of the computational domain allows researching how changes in the shape of hydrocyclone will influence its operating performance. Other developments will focus on the incorporation of turbulence models in 3D.

A more thorough investigation of the algorithm presented here is necessary and some complementary work to verify and validate numerical solutions has been undertaken. This model will be examined through experimental testing. The more advanced computations may exceed the current workstation capabilities. However, the availability of modern supercomputers allows the approximation of 3D multiphase flows in hydrocyclones to be attempted.

Appendix A

Let S denote the collection of all realisations of the motion of the mixture in D subject to certain initial and boundary conditions. Let 'm' be a proper measure on S and φ be the probability density function on S such that:

$$\int_S \varphi(s)\, \mathrm{d}m(s) = 1 \tag{A1}$$

Corresponding to each realisation $s \in S$, there exist:

(1) A solid particle constituent distribution function $\chi_{\mathrm{i}}(\boldsymbol{x}, t, d_{\mathrm{i}}; s)$ in $\mathsf{D}\times[0,\infty)$ with

$$\chi_{\mathrm{i}}(\boldsymbol{x},\ t,\ d_{\mathrm{i}},\ s)=\begin{cases}1, \text{ if } \boldsymbol{x} \text{ is occupied by particle with } d_{\mathrm{i}} \text{ at } t\\ 0, \text{ otherwise}\end{cases} \tag{A2}$$

(2) An interface distribution function $\chi_{\mathrm{I}}\ (\boldsymbol{x}, t, d_{\mathrm{i}}; s)$ in $\mathsf{D}\times[0,\infty)$with

$$\chi_{\mathrm{I}}(\boldsymbol{x},\ t,\ d_{\mathrm{i}},\ s)=\begin{cases}1, \text{ if } \boldsymbol{x}\in I(t;\ s)\\ 0, \text{ otherwise}\end{cases} \tag{A3}$$

where $I(d; s)$:=cl $\{\boldsymbol{x}\in\mathsf{D}\text{:}\quad \chi(\boldsymbol{x}, t, d_{\mathrm{i}}; s)=1\}\bigcap$cl$\{\boldsymbol{x}\in\mathsf{D}\text{:}\ \chi(\boldsymbol{x}, t, d_{\mathrm{i}}; s)=0\}$ is the interface between the fluid constituent and the solid constituent,

(3) A mass density field function

$$\tilde{\rho}(\boldsymbol{x},\ t,\ d_{\mathrm{i}};\ s) \text{ in } \mathsf{D}\times[0,\ \infty) \tag{A4}$$

(4) A velocity field

$$\tilde{\boldsymbol{v}}(\boldsymbol{x},\ t,\ d_{\mathrm{i}};\ s) \text{ in } \mathsf{D}\times[0,\ \infty) \tag{A5}$$

The interface $I(d; s)$ is singular, across which ? has a jump and on which ρ and χ may not be defined.

From χ and ρ, the mass density distribution ρ_{f} and ρ_{pi} associated with $s\in S$ can be obtained,

$$\tilde{\rho}_{\mathrm{f}}=\rho\left(1-\sum_{i=1}^{i=N}\chi\ (\boldsymbol{x},\ t,\ d_{\mathrm{i}};\ s)\right) \tag{A6}$$

$$\tilde{\rho}_{\mathrm{i}}=\tilde{\rho}\chi(\boldsymbol{x},\ t,\ d_{\mathrm{i}};\ s). \tag{A7}$$

The velocity field $\tilde{\boldsymbol{v}}_{\mathrm{f}}$ of the fluid constituent and the velocity field $\tilde{\boldsymbol{v}}_{\mathrm{i}}$ of the solid constituent are given by:

$$\tilde{\boldsymbol{v}}_{\mathrm{f}}=\tilde{\boldsymbol{v}} \text{ on } \mathsf{D}_{\mathrm{f}}=\{\boldsymbol{x}\in\mathsf{D}\text{:}\ \chi_{\mathrm{i}}(\boldsymbol{x},\ t,\ d_{\mathrm{i}};\ s)=0\} \tag{A8}$$

$$\tilde{\boldsymbol{v}}_{\mathrm{i}}=\tilde{\boldsymbol{v}} \text{ on } \mathsf{D}_{\mathrm{i}}=\{\mathbf{x}\in\mathsf{D}\text{:}\ \chi_{\mathrm{i}}(\boldsymbol{x},\ t,\ d_{\mathrm{i}};\ s)=1\} \tag{A9}$$

A particle group 'i' volume fraction:

$$\alpha_{\mathrm{i}}:=\int_S\chi_i(x,\ t,\ d_{\mathrm{i}};\ s)\varphi(s)\,\mathrm{d}m(s) \tag{A10}$$

A fluid density

$$\rho_{\mathrm{f}}:=\int_S\tilde{\rho}\left(1-\sum_{i=1}^{i=N}\chi_{\mathrm{i}}\ (\boldsymbol{x},\ t,\ d_{\mathrm{i}};\ s)\right)\varphi(s)\,\mathrm{d}m(s) \tag{A11}$$

A momentum of a particle group 'i'

$$\rho_{\mathrm{i}}\boldsymbol{v}_{\mathrm{i}}(\boldsymbol{x},\ t):=\int_S(\tilde{\rho}\tilde{\boldsymbol{v}})\chi_{\mathrm{i}}(\boldsymbol{x},\ t,\ d_{\mathrm{i}};\ s)\varphi(s)\,\mathrm{d}m(s) \tag{A12}$$

A momentum of the fluid:

$$\rho_{\mathrm{f}}\boldsymbol{v}_{\mathrm{f}}(\boldsymbol{x},\ t):=\int_S(\tilde{\rho}\tilde{\boldsymbol{v}})\left(1-\sum_{i=1}^{i=N}\chi_{\mathrm{i}}\ (\boldsymbol{x},\ t,\ d_{\mathrm{i}};\ s)\right)\times\varphi(s)\,\mathrm{d}m(s) \tag{A13}$$

The physical fields for the motion of the solid phases are not continuous in space and in time. Therefore, the concept of Reynolds' decomposition scheme for a one phase flow, cannot be applied here. Rajagopal and Tao [9] defined the correlations for the fluctuating velocities in the following way:

$$(\rho_{\mathrm{f}}\overline{\acute{\boldsymbol{v}}_{\mathrm{f}}\acute{\boldsymbol{v}}_{\mathrm{f}}})(\boldsymbol{x},\ t):=\int_S\left[\tilde{\rho}\left(1-\sum_{i=1}^{i=N}\chi_{\mathrm{i}}(\boldsymbol{x},\ t,\ d_{\mathrm{i}};\ s\right)\right]\times\left[\tilde{\boldsymbol{v}}\ (\boldsymbol{x},\ t,\ d_{\mathrm{i}};\ s)-\boldsymbol{v}_{\mathrm{f}}(\boldsymbol{x},\ t)\right]\otimes\left[\tilde{\boldsymbol{v}}(\boldsymbol{x},\ t,\ d_{\mathrm{i}};\ s)-\boldsymbol{v}_{\mathrm{f}}(\boldsymbol{x},\ t)\right]\varphi(s)\,\mathrm{d}m(s) \tag{A14}$$

$$(\rho_{\mathrm{f}}\overline{\acute{\boldsymbol{v}}_{\mathrm{f}}\acute{\boldsymbol{v}}_{\mathrm{f}}})(\boldsymbol{x},\ t):=\int_S\left[\tilde{\rho}\chi_{\mathrm{i}}\ ((\boldsymbol{x},\ t,\ d_{\mathrm{i}};\ s))\right]\times\left[\tilde{\boldsymbol{v}}(\boldsymbol{x},\ t,\ d_{\mathrm{i}};\ s)-\boldsymbol{v}_{\mathrm{i}}(\boldsymbol{x},\ t)\right]\otimes\left[\tilde{\boldsymbol{v}}(\boldsymbol{x},\ t,\ d_{\mathrm{i}};\ s)-\boldsymbol{v}_{\mathrm{i}}(\boldsymbol{x},\ t)\right]\varphi(s)\,\mathrm{d}m(s) \tag{A15}$$

References

[1] M. Nonaka, H. Tashiro, Turbulent transport effect on hydrocyclone performance, J. Environ. Eng. 122 (4) (1996) 306.

[2] T. Dyakowski, R.A. Williams, Modelling turbulent flow within a small-diameter hydrocyclone, Chem. Eng. Sci. 48 (1993) 1143.

[3] K.T. Hsieh, K. Rajamani, Phenomenological model of the hydrocyclone: model development and verification for single-phase flow. Int. J. Miner. Process 22 (1988) 223.

[4] M.I.G. Bloor, D.B. Ingham, The flow in industrial cyclones, J. Fluid Mech. 178 (1987) 507.

[5] J. Averous, R. Fuentes, Advances in the numerical simulation of hydrocyclone classification, Can. Metall. Q. 36 (5) (1997) 309.

[6] B. Devulapalli, R.K. Rajamani, in: D. Claxton, L. Svarovsky, M. Thew (Eds.), A comprehensive CFD model for particle-size classification in industrial hydrocyclones, Hydrocyclones-96, Mechanical Engineering, London, UK, 1996.

[7] M.R. Davidson, A numerical model of liquid–solid flow n a hydrocyclone with high solids fraction: FED-185, Numerical Methods Multiphase Flows ASME (1994) 29.

[8] C.T. Crowe, M. Sommerfeld, Y. Tsuji, Multiphase flows with droplets and particles, CRC Press, Boca Raton, FL, 1998.

[9] K.R. Rajagopal, L. Tao, Mechanics of Mixtures, Series on Advances in Mathematics for Applied Sciences, vol. 35, World Scientific, Singapore, 1995.

[10] M.C. Roco, In: P.N. Cheromisirioff (Ed.), Gulf Publ. Co., Hanston, TX (1990) One Equation Turbulence Modelling of Incompressible Mixtures: Encyclopedia of Fluid Mechanics, 10, Surface and Ground Water Flow Phenomena, Cheremisinoff, 1990, p. 1.

[11] R.K. Rajamani, L. Milin, in: L. Svarovsky, M. Thew (Eds.), Fluid-Flow Model of the hydrocyclone for concentrated slurry classification: Hydrocyclones Analysis and Applications, Kluwer Academic, UK, 1992, p. 95.

[12] F. Concha, A. Barrientos, L. Munoz, O. Bustamante, O. Castro, D. Claxton L. Svarovsky M. Thew (Eds.), Phenomenological Model of a Hydrocyclone, Hydrocyclone-96 (1996) 63Mechanical EngineeringLondon, UK.

[13] P.M. Gresho, Incompressible fluid dynamics: some fundamental formulation issues, Annu. Rev. Fluid Mech. 23 (1991) 413.

[14] M.D. Gunzburger, Finite Element Method for Viscous Incompressible Flow, Academic Press, San Diego, 1989.

[15] R.L. Sani, P.M. Gresho, R.L. Lee, D.F. Griffiths, The cause and cure (?) of the spurious pressures generated by certain FEM solutions of the incompressible Navier–Stokes equations: Part 1, Int. J. Numerical Methods Fluids 1 (1981) 17.
[16] R.L. Sani, P.M. Gresho, R.L. Lee, D.F. Griffiths, The cause and cure (?) of the spurious pressures generated by certain FEM solutions of the incompressible Navier–Stokes equations: Part 2, Int. J. Numerical Methods Fluids 1 (1981) 171.
[17] F. Brezzi, M. Fortin, Mixed and Hybrid Finite Element Methods, Springer-Verlag, Berlin, 1991.
[18] R.W. Thatcher, The Finite element method for three dimensional incompressible flow, Incompressible Comput. Fluid Dyn. 13 (1993) 427.
[19] V. Haroutunian, M.S. Engelman, I. Haasbani, Segregated finite element algorithms for the numerical solution of large-scale incompressible flow problems, Int. J. Numerical Methods Fluids 17 (1993) 323.
[20] S.V. Patankar, Numerical Heat transfer and Fluid Flow, Hemisphere, Washington, DC, 1980.